Steady-State and Decay Dynamics for Impellers of Varying Aspect Ratio in Unbaffled Tanks

D. Maynes and M. Butcher
Dept. of Mechanical Engineering, 435 CTB, Brigham Young University, Provo, UT 84602

Hydrodynamic torque measurements on impellers of square cross section were conducted for 33 different impellers in 3 different cylindrical unbaffled tanks. The tanks differed in volume by two orders of magnitude, and the Reynolds number range of the data was $10^4 - 10^5$. A wide range of impeller sizes and aspect ratios was investigated, focusing on the decay regime where the tank walls impacted the torque measurement, and the steady state where the torque is constant on average. The number of revolutions required for spin-up to steady state is a function of the tank radius and height and the impeller radius and height, and an expression is presented that describes the spin-up time in terms of these variables and is valid for all of the data. At steady state and for a Reynolds number of 10^5, the torque coefficient or power number depended primarily on the height of the impeller and tank, but not on the impeller radius. During the decay regime, the measured torque coefficient decreases with a power-law relation and is proportional to the number of revolutions raised to the k power. The k value did not depend on the height of the tank, but only on the impeller radius, impeller height, and tank radius. Expressions relating the steady-state torque coefficient and the decay exponent, k, to the geometric variables model all of the data quite well. With these relations, the effects of the varying impeller aspect ratios on the energy required for mixing of momentum, and on the time required for mixing to occur, can be quantified.

Introduction

For spin-up of a bluff body (square impeller) from rest in an initially quiescent fluid contained in a cylindrical tank, three distinct temporal regimes are observed (Maynes et al., 1998, 1999). The first regime has been termed the buildup regime. In this regime, the hydrodynamic torque on the bluff body and the velocity fluctuations of the tangential velocity in the bulk flow remain relatively constant. The effects of the tank walls have not yet affected the flow near the body, and the behavior is similar to what would occur if the body rotated in an infinite fluid. The second regime was termed the decay regime. In this regime, the torque and velocity fluctuations decay with power-law relations. The decay of the torque and the velocity fluctuations occur because, after some characteristic time, the effects of the tank walls impact the flow behavior near the rotating body. Decay continues until steady state is reached, which is the third regime. At steady state, the average torque and the velocity fluctuations level off to approximately constant values. In this regime, the momentum added to the fluid by the rotating body is balanced by the destruction of momentum at the tank walls.

Aside from the works just cited, most of the previous work related to bluff-body flows has been in the broad area of stirred mixing tank flows. Many investigations concerning the mixing of liquids in stirred tanks are available in the literature. Oldshue (1969) gives a list of many of the early works, and several of the later investigations are listed by King et al. (1988). A somewhat standard geometry for stirred mixing tanks operating in the turbulent regime was adopted by the early 1960s and continues to exist as the standard. Consequently, much of the literature addressing power requirements in stirred tanks has focused on impeller and tank geometries similar to this standard. One of the early works that was conducted by Rusthon et al., wherein they reported

Correspondence concerning this article should be addressed to D. Maynes.

(1950a,b) on a large study that quantified the power numbers for several different impeller geometries, including both axial and radial flow types. Their data covered a Reynolds number range from 1 to 10^6, and they investigated impellers rotating in both baffled and unbaffled tanks. Their work represents one of the first studies to cover such a large range of *Re* using fluids with vastly different viscosities. However, significant variations in impeller geometrical ratios, or tank-size ratios, were not explored. Later studies focused on impeller and tank geometry. These include work by Nienow and Miles (1971), who reported on power numbers for 6-blade disk turbines, 2-blade flat paddles, and 4-blade 45° pitch impellers for Reynolds numbers in the range $2\times10^4-10^5$. Specifically, this study focused on the impeller clearance above the tank bottom. Bertrand et al. (1980) also reported on power numbers for baffled tank turbulent flow conditions. They reported results for five different agitation systems and summarize power-number results from several previous studies with similar configurations. Bujalski et al. (1987) reported on the dependency of scale on power numbers for Rushton disk turbines, with specific emphasis on the thickness of the turbine disk on the measured power. Other investigators have reported on the effects of paddle dimensions and baffle conditions on the power number, in addition to mixing times (Sano and Usui, 1987), effects on the power number of altering the tank geometry to a square vessel (Papastefanos and Stamatoudis, 1989) and by changing the classic flat-bottom design to a profiled shaped (Chudacek, 1985), power numbers for impellers used in solid suspensions (Tiljander and Theliander, 1993), power consumption associated with Boger fluids (Oliver et al., 1984), and characteristics of dual Rushton impellers in stirred tanks (Rutherford et al., 1996). As noted by Ibrahim and Nienow (1995), however, "Though considerable Power number data are available in the literature, there are few results for nonstandard conditions." Indeed, for most studies in the literature the aspect ratio (impeller height/impeller radius) range has been limited to between 0.32 and 0.50. Also, the ratios of impeller radius to tank radius and impeller height to tank height are typically between 0.33 and 0.5, and 0.05 and 0.07, respectively (Tatterson, 1991). In addition, most studies have focused on unidirectional rotation without addressing the spin-up transient.

Previous rotating-bluff-body studies by Maynes et al. (1998, 1999) are important with regard to the evolution of the flow field from rest. They also led in the development of a time scaling that described the temporal evolution of the flow field. However, this previous work presented measurements for only seven bluff bodies in a single-sized tank and the aspect ratio (body height/body radius) range of all bodies employed was minimal. Thus the focus of this article is to present results that quantify the behavior of the torque, or power, over a large range of aspect ratios, body-radius-to-tank-radius ratio, body-height-to-tank-height ratio, and for three very different-sized tanks. The body aspect-ratio range explored is 0.35–15.89, the body-radius-to-tank-radius ratio ranges from 0.13 to 0.67, and the body-height-to-tank-height ratio is between 0.06 and 0.625. In comparison to the values shown earlier, for the traditionally studied stirred mixing tank flows, these ranges are much greater and provide a more general understanding of rotating bluff-body flows. Thus this study gives insights into the global variations in mixing dynamics when varying the aspect ratio and when varying the impeller size with respect to the tank of interest. All of our present results correspond to a Reynolds number range of 10^4-10^5. Specifically, this article focuses on the decay and steady-state regimes or the rotation period after the effects of the tank walls have impacted the flow field. A similar article reports on the buildup regime dynamics (Maynes and Butcher, 2001). Insight into how the flow field, during steady state and the decay period, depends on the parameters given earlier is addressed. Also a time scale that describes the spin-up transient, and in general for all bodies and tanks employed, is presented. In practice this work's significance is in its descriptions of the time required for resuspension of solids after shutdown of a stirred-tank process.

Methodology

Tank sizes and bodies employed

Experiments were conducted in three different tanks, the radiuses of the tanks were $R = 0.457$ m, 0.294 m, and 0.105 m. The corresponding heights for these tanks, and the tank aspect ratios, were $H = 1.52$ m ($H^* = H/R = 3.33$), 0.42 m ($H^* = 1.43$), and 0.254 m ($H^* = 2.42$).

Solid rectangular blocks were utilized as impellers and represent the simplest geometry that produces a wake when rotated. The characteristic length, L, of the bluff bodies utilized was defined to be the body radius, or distance from the center of the body out to a corner in a horizontal plane. The aspect ratio of the body is the ratio of the body height, h, over L. In the small tank ($H^* = 2.42$), 10 different bluff bodies were used, ranging in aspect ratio from 0.42 to 2.83, with L values of 0.041–0.071 m ($L^* = L/R = 0.39$–0.68). In the medium tank ($H^* = 1.43$), 14 bluff bodies were used. These bodies varied in aspect ratio from 0.35 to 4.24, where L varied from 0.041 to 0.11 m ($L^* = 0.14$–0.374). In the large tank ($H^* = 3.33$), 7 bodies were used, ranging in aspect ratio from 0.71 to 15.9, with L varying between 0.06 and 0.32 m ($L^* = 0.13$–0.67). All of the bodies were square in cross section. Table 1 lists the bluff bodies used, the dimensions for each, the Reynolds number range ($Re = \Omega L^2/\nu$) for each, and the tank in which it was used. The fluid used was water at approximately 20°C for all of our present data. Also, for all experiments, the tank was completely filled so that a free surface did not exist.

Table 1. Body Specifications and *Re* Ranges Explored

L^*	h/L	*Re* Range
Small tank ($R = 0.105$ m, $H = 0.254$ m, $H^* = 2.42$)		
0.67	0.42, 0.99, 1.41, 1.84, 2.26	$3.1\times10^4-2.8\times10^5$
0.39	0.56, 1.14, 1.4, 2.83, 4.25	$4.8\times10^4-2.2\times10^5$
Medium tank ($R = 0.294$ m, $H = 0.42$ m, $H^* = 1.43$)		
0.36	0.35, 0.71, 1.41, 1.89	$2.5\times10^4-2.6\times10^5$
0.24	0.42, 0.99, 1.41, 1.84, 2.26	$2.5\times10^4-2.6\times10^5$
0.14	0.56, 1.13, 1.41, 2.83, 4.24	$2.5\times10^4-1.5\times10^5$
Large tank ($R = 0.457$ m, $H = 1.52$ m, $H^* = 3.33$)		
0.13	15.89	$1\times10^3-1\times10^4$
0.15	6.83	$9\times10^3-9\times10^4$
0.22	1.65, 4.55	$2\times10^4-1.5\times10^5$
0.31	0.71, 141	$2.5\times10^4-2.8\times10^5$
0.37	2.73	$4\times10^4-2.6\times10^5$
0.67	0.94	$6\times10^4-5.8\times10^5$

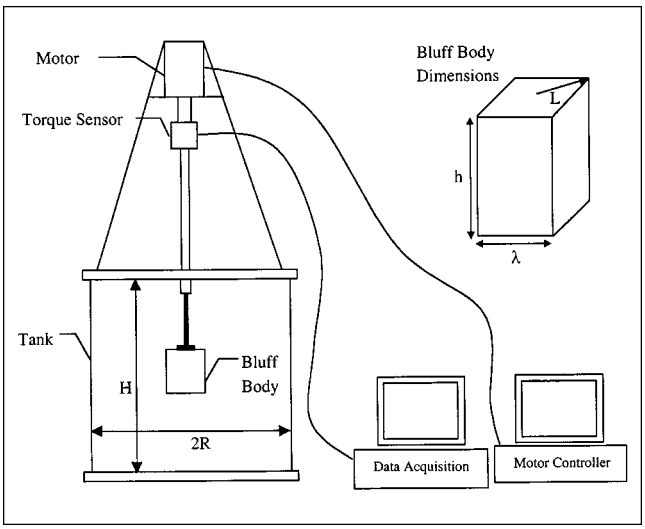

Figure 1. Experimental facility along with characteristic impeller and tank dimensions.

The impellers are solid rectangular blocks.

Experimental setup

Figure 1 shows the experimental setup and a typical bluff body. Regardless of the body or tank used, data acquisition was similar for all tests. The body was connected to a stepper motor, controlled by a Macintosh computer, via a shaft, and located such that the center of the body coincided with the center of the tank. An in-line torque sensor that interfaced with a data-acquisition system was mounted on the shaft between the body and the motor. After the fluid in the tank had completely come to rest, motion and data acquisition were initiated. Data were acquired for a time much longer than the time required for steady state to be attained. The acquisition rate was 100 Hz for all of the experiments, and this sampling frequency was much greater than double the largest frequencies resolved by the sensor, due to fluid motions. The maximum rotation rate for each body was limited by the loading limits of the torque sensors employed.

The motor utilized was an SX Series Compumotor manufactured by Parker Hannifin Corporation. It consisted of a programmable indexer and drive connected with a stepper motor, and it allowed the acceleration, rotation rate, and number of revolutions to be specified. According to the manufacturer's specifications, the accuracy of the velocity and acceleration were within 0.02%.

Two key-transducer torque meters were employed to obtain the torque measurements in the experiments. The transducers were mounted in line with the bluff-body impellers via couplers and the sensor housing was fixed, thus nonrotating. The transducer shaft is strain gauged using resistive strain gauges, and the gauges are placed in a Wheatstone bridge configuration, that is excited at 3.28 kHz. The resultant signal voltage from the bridge is transmitted via a wideband linear transformer to a signal conditioner. The signal is low-pass filtered in the signal conditioner at 400 Hz. The actual sampling rate was 100 Hz, and is sufficient to capture the dynamics of the spin-up process for even the fastest evolving flow studied. This corresponds to the case of $L^* = 0.67$ in the small tank ($H^* = 2.42$) with a rotation rate of 3.67 revolutions/s. For this case, the buildup regime (the shortest temporal regime) lasts about 0.5 s, and using a sampling frequency of 100 Hz, results in 50 data points, which is sufficient to characterize this regime. The output from the transducers is a voltage signal with values between -5 and 5 V and, as specified by the manufacturer and the accuracy, is $\pm 0.05\%$ of full scale. For the sensor used in the small and medium tanks, full scale corresponded to a torque value of 0.706 N-m. This sensor was also utilized in the large tank in addition to a second sensor, where full scale corresponds to 22.6 N-m.

The signal from the transducer was connected to an A/D converter interfaced with a PC machine. The motor and acquisition program were initiated by the same trigger switch, and when the switch was closed, the data-acquisition system began collecting data and the motor began to rotate. The data-collection process stopped shortly before the motor ceased rotating. All of the experiments were conducted in the following manner. The fluid was allowed to come to rest prior to initiation of rotation. Motion was initiated and the data-acquisition system was triggered by the rotational motor drive. Rotation continued until the mean-flow steady-state condition was maintained long enough to reliably quantify the mean-flow steady-state torque.

For each set of data, the resulting torque is a combination of the hydrodynamic torque, torque required to overcome inertia in the ramp up to constant ω, and torque required to overcome friction in the shaft bearings. For all cases presented, the torque to overcome inertia is small and only of concern in the acceleration region. This is because the inertia of the bodies is small and high accelerations were not used. For the highest α and largest body used, the torque required to overcome inertia was only about 1% of the maximum torque in the acceleration period. The bearing-friction torque was quantified by measuring the torque with the tank empty. These measurements were very repeatable with different sizes of bodies mounted to the shaft. As expected, it was found that the friction torque was only a function of rotational velocity and the magnitude was, in all cases, very small compared to the hydrodynamic torque.

Nondimensional parameters

For fast accelerating flow the hydrodynamic torque can be written as $T = T(L, R, H, h, \omega, \nu, \rho, t)$, where T is the torque, L is the characteristic length of the body, h is the height of the body, R is the radius of the tank, H is the height of the tank, ω is the rotation rate in radians/s, ν is the kinematic viscosity, ρ is the fluid density, and t is time. Standard dimensional analysis reduces the number of variables from nine to six. The following nondimensional parameters describe the flow field from startup

$$C_m = \frac{T}{\frac{1}{2}\rho\omega^2 L^4 h} \tag{1}$$

$$Re = \frac{\omega L^2}{\nu} \tag{2}$$

$$L^* = \frac{L}{R} \tag{3}$$

$$h^* = \frac{h}{R} \tag{4}$$

$$H^* = \frac{H}{R} \tag{5}$$

$$t^* = \frac{\omega t}{2\pi}, \tag{6}$$

where C_m is the nondimensional torque coefficient, Re is the Reynolds number, t^* is the number of revolutions, and L^*, h^*, and H^* are geometric parameters for the body and tank. Values for the density and kinematic viscosity were obtained for water at 20°C. Note that C_m has the same form as, and can be thought of as a power number that is traditionally used in mixing-tank literature. For this study and all of our computations the rotation rate has been expressed in rad/s.

Error Analysis

The primary source of error in the experiments was associated with the torque sensor employed. The output signal from both transducers was accurate to within $\pm 0.05\%$ of full scale. This corresponds to bias errors of $\pm 3.53\times10^{-4}$ N·m and $\pm 1.12\times10^{-2}$ N·m for the small and large sensors, respectively. There was also some precision error in the torque measurement due to the electrical noise in the voltage signal. During the buildup and steady-state regimes, computing the average torque over several data points minimized the precision error. Using standard error analysis the maximum precision error for the small sensor was computed to be 0.0006 N·m. The total error from the torque measurement was then determined.

The density was determined by looking it up in a table at the given temperature and was assumed to be accurate to within 0.5 kg/m^3. According to the manufacturer specifications on the motor, the rotation rate was accurate to within $\pm 0.02\%$ of the rotation rate. The scale used to measure the characteristic length and height has a least count of 1 mm. These measurements were assumed to be accurate to within 0.5 mm. The value of C_{me}, the uncertainty in determining C_m, was calculated for each data set. The maximum error was associated with the smallest body at the lowest rotation rate during the steady-state regime. This was calculated to be 12.5%. The error for the rest of the measurements ranged from 1 to 10%, with almost all of the measurements being accurate to within $\pm 5\%$.

Overview of the Spin-Up Process

Figure 2 shows a sample of the data collected for a body in the medium tank with $L^* = 0.24$ and $h/L = 1.41$. This figure plots C_m vs. the number of revolutions, t^*, for three different Re. The data illustrate the three distinct temporal regimes that exist. The buildup regime, where the value of the C_m remains relatively constant, corresponds to $1 \le t^* \le 20$. The decay regime, where C_m decays with a power-law relation, corresponds to $20 \le t^* \le 200$. And the steady-state regime, where the torque levels off to a constant mean value, corresponds to $t^* > 200$. The results presented in this article focus on the effects of body aspect ratio and tank geometry on C_m during the decay and steady-state regimes and on the characteristic time scale associated with the spin-up process.

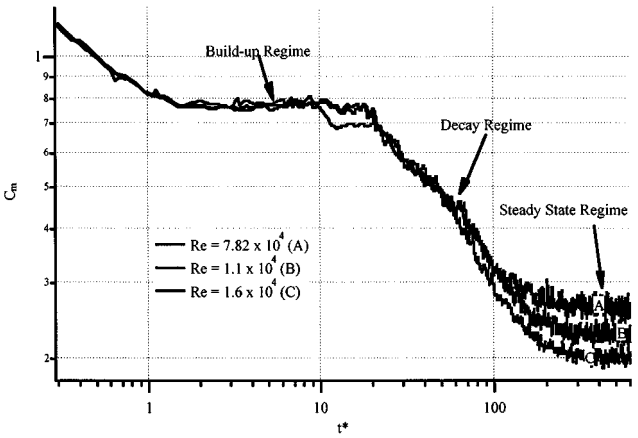

Figure 2. Torque coefficient, C_m vs. number of revolutions, t^*, for $L^* = 0.24$ and $h/L = 1.41$ in the medium tank ($H^* = 1.43$) at Reynolds numbers of 7.82×10^4, 1.1×10^5 and 1.6×10^5.

This figure illustrates the three temporal regimes that exist in the spin-up from rest to steady state of a rotating impeller.

When a body begins to rotate, there is an initial inertial loading that causes the values of the torque to quickly reach a peak. After the body ceases to accelerate, the value of the torque levels off to an approximately constant value. The buildup regime lasts from the time that this constant value is reached until the torque begins to decrease. When the body first begins to rotate, a starting vortex is formed on the leeside of each corner as viewed in the r-θ plane. These initial vortices are shed from the body and convect out into the bulk-flow region. After the initial vortex is ejected, a separation region is observed to exist and remain on the leeside of each corner. Also because of the low pressure that exists in these separation zones, a secondary flow is induced by the body rotation. On average the secondary motion is toward the midplane above and below the body and radially outward at the midplane (often called impeller stream).

It is this secondary flow that accounts for much of the transport of momentum throughout the tank. Initially the fluid that is transported by the secondary flow into the region near the body has little or no angular momentum associated with it until it is acted on by the body. As long as this is the case, the torque on the body must remain relatively constant, because the size of the recirculation, and thus low pressure, regions do not change. This is the condition that would exist if the body were to rotate in an infinite medium. Because the flow is confined, fluid that has been acted on by the body, either directly or indirectly, is transported by the secondary flow back to the region either above or below the body. At this time the fluid now transported into the region near the body is again acted upon. However, now the relative velocity between fluid and object is smaller, leading to smaller recirculation and low-pressure regions. Consequently, the torque begins to decrease. As rotation continues, the torque decays

until a condition is reached where the destruction of momentum at the tank walls, due to the wall boundary layers, is balanced by the addition of momentum by the rotating body. Also at this time, the power input must equal the rate of energy dissipation.

The behavior of fluctuations in the velocity field is very similar to the torque data. During the buildup regime the representative velocity fluctuations about a mean, or velocity rms termed v', are approximately constant. This is followed by a power-law decrease in the decay regime, and the steady-state condition where v' is relatively constant. A limited amount of v' vs. time data has been presented previously (Maynes et al., 1999), and it was shown that C_m is proportional to $v^{*2} = v'^2/(\omega L)^2$ throughout the spin-up process. During decay, $C_m \sim t^{-k}$ and $v \sim t^{-k/2}$. That C_m and v^* are related in this manner makes physical sense, because it is the relative velocity between the body and the fluid that is important with regard to the required torque and the velocity scale of the characteristic turbulent eddies.

Based on the preceding quantitative description of the flow-field dynamics, it would be expected that the only important parameters affecting the value of C_m in the buildup regime are the body dimensions. The tank dimensions clearly are important with regard to the time over which the buildup regime behavior exists; however, with regard to the magnitude of the torque, they should not be significant. Indeed our measurements show that C_m during the buildup regime is only dependent upon the h/L ratio (Maynes and Butcher, 2001). During decay and steady state, however, both the tank and body geometries are important. The results from all of our experiments quantify the effects of varying L^*, h^*, H^*, and Re with regard to (1) the elapsed number of revolutions until steady state is reached; (2) the value of C_m at steady state; and (3) the rate of decay of C_m during the decay regime. These results are presented below.

Characteristic Steady-State Time Scale

Aspect ratio and Reynolds numbers effects on the spin-up time

At a certain t^* after initiation of rotation, C_m levels off to a value that on average remains constant until the rotation parameters are changed. For example, for the data of Figure 2, the t^* is about 280 when steady state is attained. To determine this value, the average value of C_m for $400 < t^* < 2000$ was first computed. Then a least-square polynomial was fit to the data between $200 < t^* < 400$. Finally, the value of t^* when the curve fit reached a value within 2% of the steady state value of C_m was determined and was designated the number of revolutions to spin-up (280 for this case). In this manner we determined the spin-up time for all of the cases investigated. Our data show that for a given body and tank geometry, the spin-up value of t^* is largely independent of Re; however, it is strongly dependent on L^*, h^*, and H^*.

Shown in Figure 3 is the spin-up value of t^* plotted vs. the aspect ratio, h/L, for three L^* (0.14, 0.24, 0.36) in the $H^* = 1.43$ tank and for two L^* (0.39, 0.67) in the $H^* = 2.42$ tank. As the data show, the spin-up t^* decreases as h/L increases for fixed L^*. Indeed, the trend in the data appears to be a decrease in t^* by about 50% given a doubling of h/L, and the relation appears to be a power-law form ($t^* \sim [h/L]^{-c}$),

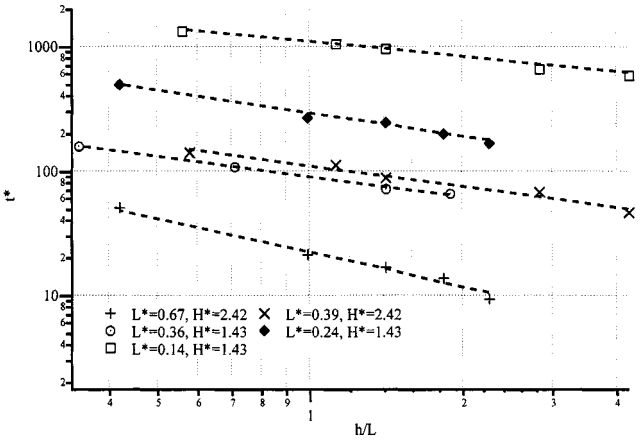

Figure 3. Number of revolutions, t^*, until steady state is attained vs. h/L at $Re = 10^5$ for $L^* = 0.14$, 0.24, and 0.36 in the medium tank ($H^* = 1.43$), and $L^* = 0.39$ and 0.67 in the small tank ($H^* = 2.42$).

where c is some constant. Variations in L^* have an even larger effect on the spin-up time, where the spin-up t^* decreases for increasing L^* with h/L fixed. With $h/L = 1.41$, t^* for spin-up is about 17 for $L^* = 0.67$ ($H^* = 2.42$), 72 for $L^* = 0.36$ ($H^* = 1.43$), 90 for $L^* = 0.39$ ($H^* = 2.42$), 240 for $L^* = 0.24$ ($H = 1.43$), and 950 for $L^* = 0.36$ ($H^* = 1.43$). Note that increasing H^* (tank aspect ratio) also results in an increase in the spin-up, t^*, as evidenced by the $L^* = 0.36$ ($H^* = 1.43$) and the $L^* = 0.39$ ($H^* = 2.42$) sets of data.

Tank-size effects and generalized spin-up time scaling

The preceding observations about variations in the spin-up t^* with L^*, h/L, and H^* are all quite intuitive. They indicate that as the tank volume increases, the spin-up time increases, and as the body size increases, the spin-up time decreases. However, a quantitative expression predicting spin-up in terms of these parameters is important.

Based on standard turbulent flow scaling the time required for transport over distance in a fluid can be expressed as $t_x \sim l_x^2/D_t$, where l_x is a characteristic length over which turbulent motions are convected and D_t represents a turbulent diffusivity; D_t should scale with the product of the characteristic velocity of the dominant turbulent motions and the characteristic length scale of these motions. The velocity of these motions should scale with the driving velocity in the tank, ωL, and the length scale of these motions should be proportional to the characteristic length of the body from which they are generated, L. Thus the turbulent diffusivity should scale as $D_t \sim \omega L^2$. The time for turbulent motions to convect over the entire tank volume should thus be $t_x \sim l_x^2/(\omega L^2)$, where l_x represents an appropriate length describing the tank size. Normalizing the actual time, t, by t_x, we can write a nondimensional time scale as $\tau \sim t\omega L^2/l_x^2$, or for fast accelerating flows

$$\tau \sim t^* \frac{L^2}{l_x^2}. \tag{7}$$

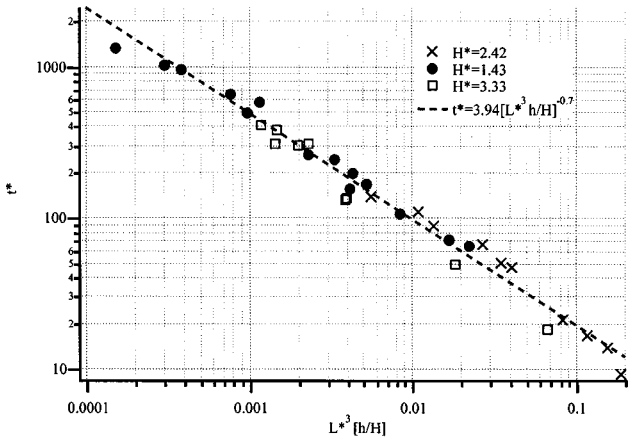

Figure 4. Number of revolutions, t^*, until steady state is attained at $Re = 10^5$ vs. $L^{*3}[h/H]$ for all h/L utilized in the three tanks.

This expression for τ suggests the spin-up time is inversely proportional to L^2 and proportional to l_x^2, but contains no h dependence.

Shown in Figure 4 is the spin-up value of t^* plotted vs. $L^{*3}[h/H]$ for 33 different bodies and representing all three tanks. This nondimensional parameter was chosen because in so doing the data collapse to a well-behaved power-law relation where t^* decreases for increasing $L^{*3}[h/H]$. A least-square fit to the data suggests the form

$$t^*_{ss} = 3.94\left[L^{*3}\frac{h}{H}\right]^{-0.7}. \qquad (8)$$

The fit of the expression to the experimental data is very good with a correlation coefficient of 0.99 and an average difference between measurement and curve fit expression of 3.3%. After rearrangement we can write

$$3.94 = t^*\left[L^*\right]^{2.1}\left[\frac{h^*}{H^*}\right]^{0.7}. \qquad (9)$$

This is very similar to the simple scaling argument presented in Eq. 7 if $l_x = R$. The only significant differences are that the ratio of body-height to tank-height term does not appear in the scaling argument, and that L^* is raised to the power of 2.1 instead of 2, which was expected based on the physical argument given earlier. The cause of these differences is likely simply due to the complexity of developing simple scaling arguments in turbulent flows with multiple geometric length scales.

The importance of the data and curve-fit relation for t^* is that it describes the time required for momentum to be transferred over an entire tank volume for tanks ranging in volume from 8.8 l to 1000 l, for a range of L^* from 0.13 to 0.67, and for a large range of body aspect ratios (0.35–15.89). By analogy, the time required for mixing of two, or more, species in a tank using a square impeller should show similar trends. However, recall that the expression in Eq. 9 corresponds to momentum mixing undergoing spin-up from rest. For unidirectional operation experiments measuring either heat or mass transport are necessary for characterizing the mixing process. Although all of our data correspond to square impellers over a wide range of aspect ratio, the trends in the time-scaling results should be applicable to other radial flow impellers located in the center of a tank.

Steady-State Regime C_m Results

Data illustrating the effects of variations in aspect ratio, Reynolds number, and tank size on the behavior of C_m at steady state are now presented. An average of the torque signal over several revolutions was computed for each value of C_m shown.

Reynolds number and aspect-ratio effects on C_m

Shown in Figure 5 is C_m at steady-state plotted vs. Re for $L^* = 0.39$ (Figure 5a) and $L^* = 0.67$ (Figure 5b) in the $H^* =$

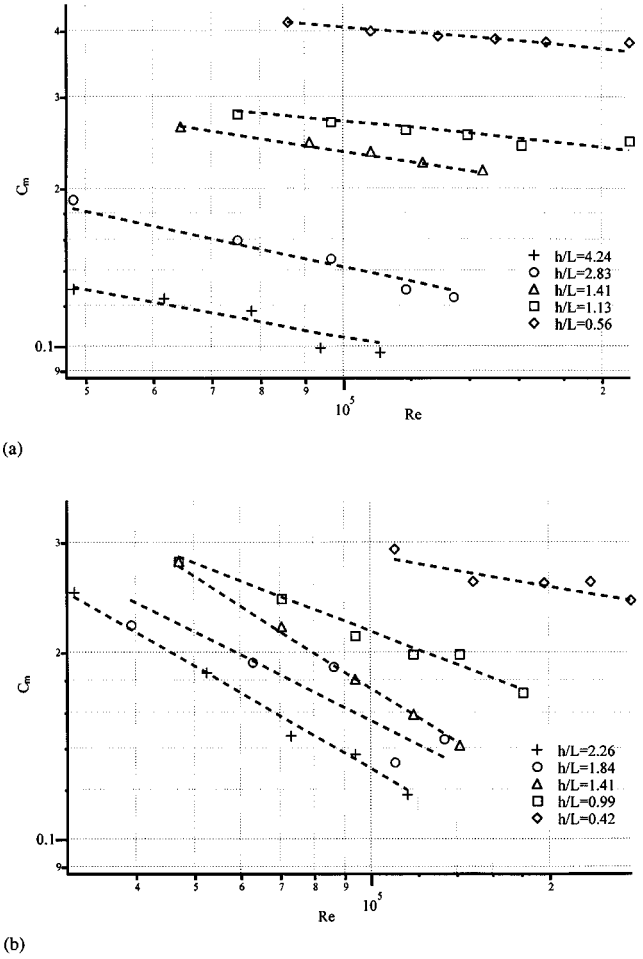

Figure 5. Steady-state value of the torque coefficient, C_m, vs. Reynolds number, Re, in the small tank ($h^* = 2.42$) for (a) $L^* = 0.39$, with h/L ranging from 0.56 to 4.24, and (b) $L^* = 0.67$, with h/L ranging from 0.42 to 2.26.

2.42 tank. For the two L^*, h/L ranges from 0.42 to 2.26 and 0.56 to 4.25, respectively. Similarly Figure 6 presents data from the $H^* = 1.43$ tank for $L^* = 0.14$ (Figure 6a), 0.24 (Figure 6b), and 0.36 (Figure 6c). For these data, the corresponding h/L ranges are 0.56–4.24, 0.42–2.26, and 0.35–1.89. Figure 7 shows data from the $H^* = 3.33$ tank for $L^* = 0.13$ ($h/L = 15.9$), 0.15 ($h/L = 6.83$) 0.23 ($h/L = 1.65$ and 4.55), 0.31 ($h/L = 0.71$ and 1.41), and $L^* = 39$ ($h/L = 2.73$). Four trends are obvious in the data of Figures 5–7 and are now discussed.

The first trend of note is that as *Re* increases, the magnitude of C_m decreases for all cases of constant L^*, H^*, and h/L. As the data show, for fixed L^*, h/L, and H^*, the decrease in C_m is proportional to Re^{-n}. This is similar to observations by early investigations of power requirements for various shaped impellers (Rushton, 1950) where the power number was observed to decrease as *Re* increases in unbaffled tanks. For tanks with baffles this was not observed, but the power number remained relatively constant over a large range of *Re*. The value of n for all of the $H^* = 3.33$ tank data ranges between 0.2 and 0.25. For the $H^* = 1.42$ tank data, n ranges from 0.1 and 0.15, and for the $H^* = 2.42$ tank with $L^* = 0.39$, n ranges from 0.15 to 0.25. For $L^* = 0.67$ in this tank, however, n appears to be greater, ranging from about 0.25 to 0.35. For these data it is evident that n is increasing as the body size (h/L) increases. This is the only case presented where $L^* \geq 0.5$, but it appears from these data that for bodies that are large in comparison to the tank, the dependence on *Re* increases. The physical reasoning for this behavior is not yet clear. From our present results the data suggest for $L^* \leq 0.5$ that n increases as H^* increases, although data from only three H^* have been presented.

The second significant trend apparent from Figures 5–7 is that, for similar L^*, *Re* and H^*, C_m decreases for increasing h/L. This is especially evident from Figures 5–6, where for each L^*, data from four to five h/L are shown, and for each case, C_m decreases with increasing h/L.

The principle force acting on a rotating bluff body is the pressure force caused by flow separation. As evident from Eq. 1, C_m is proportional to the exerted hydrodynamic torque, but is inversely proportional to h. Thus as the data indicate, increases in h, with constant L, do not result in a proportional increase in the steady-state torque. For example, for $L^* = 0.14$, $H^* = 1.42$, and at $Re = 10^5$ (Figure 6a), the magnitude of C_m is 0.16, 0.21, 0.34, 0.36, and 0.43 for $h/L = 4.24$, 2.83, 1.41, 1.13, and 0.56, respectively. The actual measured steady-state torque for each of these cases, normalized by the torque for the $h/L = 0.56$ case, ζ, is 2.82, 2.5, 1.99, 1.69, and 1.0. The corresponding ratios of body height to the height for $h/L = 0.56$, η, are 7.57, 5.05, 2.52, 2.02, and 1.0. Note that a doubling of h from $h/L = 0.56$ to 1.13 results in an increase in the torque of 1.69 times. However, an increase in h of 7.57 times, from $h/L = 0.56$ to 2.28, results in an increase in the

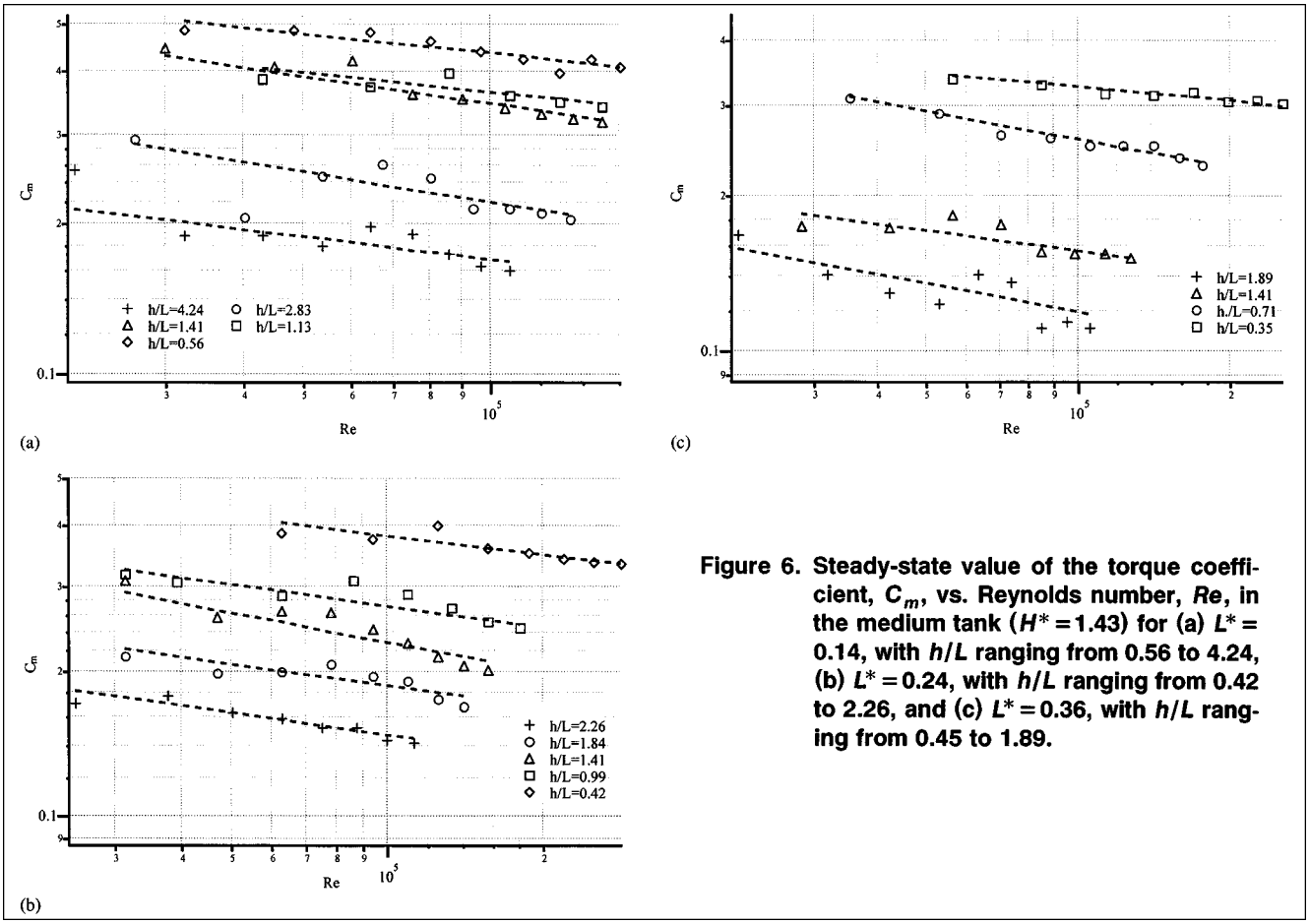

Figure 6. Steady-state value of the torque coefficient, C_m, vs. Reynolds number, *Re*, in the medium tank ($H^* = 1.43$) for (a) $L^* = 0.14$, with h/L ranging from 0.56 to 4.24, (b) $L^* = 0.24$, with h/L ranging from 0.42 to 2.26, and (c) $L^* = 0.36$, with h/L ranging from 0.45 to 1.89.

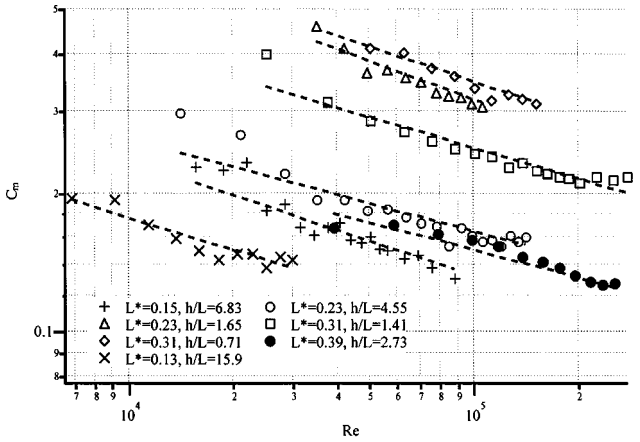

Figure 7. Steady-state value of the torque coefficient, C_m, vs. Reynolds number, Re, in the large tank ($H^* = 3.33$) for L^* ranging from 0.13 to 0.39 and h/L ranging from 0.71 to 15.9.

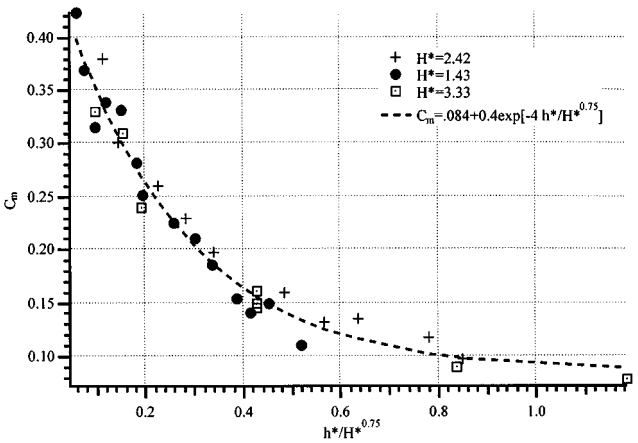

Figure 8. Steady-state value of the torque coefficient, C_m, vs. the parameter $h^*/H^{*3/4}$ at $Re = 10^5$ for all of the data shown in Figures 5–7.

torque of only 2.82 times. If ζ is plotted vs. η, for fixed L^*, Re, and H^*, the curve follows an exponential relation of the form $\zeta = A + Be^{[-E\eta]}$. Indeed our data follow an exponential relation of this form for all bodies employed in all three tanks with differing values of A, B, and E for different L^* and H^*.

The third trend of interest from Figures 5–7 is that for fixed h/L, Re, and H^*, C_m decreases for increasing L^*. This is apparent from the medium tank data where for $h/L = 1.41$ and $Re = 10^5$, C_m decreases from about 0.34 for $L^* = 0.14$, to 0.24 for $L^* = 0.24$, and finally to 0.16 for $L^* = 0.36$. Whether the variation is due to changes in L^*, as suggested by the figures, or due to corresponding changes in h, which is necessary if h/L is to remain constant, is discussed in the following subsection.

The fourth and final trend of significance from Figures 5–7 is that for similar L^*, Re, and h/L, C_m increases as H^* increases. This is evidenced by comparing the $L^* = 0.39$ and $h/L = 1.41$ data for $H^* = 2.33$ (Figure 5a) with the $L^* = 0.36$ and $h/L = 1.41$ data for $H^* = 1.42$ (Figure 6c). At $Re = 10^5$ for these two cases the value of C_m is about 0.24 for $H^* = 2.33$ and 0.16 for $H^* = 1.42$. Also for $L^* = 0.23$ and $h/L = 1.65$, C_m is about 0.30 for $H^* = 3.33$ (Figure 7), while for $L^* = 0.24$ and $h/L = 1.65$, C_m would be about 0.22 for $H^* = 1.42$ (Figure 6b). Since at steady state the torque applied to the rotating body must be equal in magnitude to the torque on the tank walls, the preceding observations make good physical sense. For a fixed L^*, Re, and h/L, increases in H^* represent an increase in the height of the tank, while all other parameters remain constant. Since this will increase the surface area over which shear forces act, the torque required for equilibrium to exist must also increase.

Generalized C_m relation at $Re = 10^5$

As noted earlier, when plotting ζ vs. η at $Re = 10^5$ the data follow the form $\zeta = A + Be^{[-E\eta]}$ for all of our present results, although for differing L^* and H^* the curves do not coincide. A similar expression describes the relation between C_m and h/L. Interestingly, when C_m is plotted vs. h^* instead of h/L, all of the data for a fixed H^* follows a single representative curve, indicating that C_m does not depend on L^*, but for fixed H^* depends only on h^*. When C_m is plotted vs. $h^*/H^{*3/4}$, all of the data from the three tanks follow a similar curve. This is illustrated in Figure 8. The data correspond to $Re = 10^5$ and include steady-state values of C_m for all 33 bodies employed in the three tanks. H^* was raised to the 3/4 power simply because the data from the three tanks tended to merge toward a single curve by doing so and 3/4 gave a better correlation than any other value.

A least-square curve of an exponential form was fit to the data of Figure 8 and is shown on the figure. The expression for the curve fit is

$$C_m \approx 0.084 + 0.4\,e^{[-4h^*/H^{*3/4}]}. \qquad (10)$$

Sixty-seven percent of the data are within 8% of this curve fit and all but one data point are within 15%. Also the correlation coefficient of the curve fit is 0.98 and the average difference between the measured data and the curve fit expression is 7%. The significance of Eq. 10 is that it describes the C_m value at steady state for a wide range of body and tank sizes, although it is limited to square impellers located in the center of a tank. Equation 10 indicates that the hydrodynamic torque is proportional to L^4; however, increases in h with fixed L result in smaller C_m values. Physically, since the torque/height is less, this indicates that the separated flow regions next to the rotating body do not increase proportionally in size as h increases. Thus, the exerted average pressure differential over the faces of the bluff body is smaller.

Decay-Regime Dynamics

Data illustrating the effects of variations in aspect ratio, Reynolds number, and tank size on the behavior of C_m during the decay regime are now presented. Note from Figure 2 that during the decay regime C_m can be expressed as $C_m \sim t^{*k}$, where k is termed the decay coefficient. This coefficient

describes the rate of decay, or the rate of spin-up, and depends on Re, L^*, h^*, and H^*. To determine k, we simply plot log (C_m) vs. log(t^*) on linear coordinates and determined the slope of the line using a least-square curve fit for each set of data. In determining this slope we used data corresponding to a t^* slightly after decay had begun to a t^* slightly before steady state was attained.

Reynolds number and aspect ratio effects on k

Results for $L^* = 0.39$ (Figure 9a) and $L^* = 0.67$ (Figure 9b) in the small tank are presented in Figure 9 and results for $L^* = 0.14$ (Figure 10a), $L^* = 0.24$ (Figure 10b), and $L^* = 0.36$ (Figure 10c) are presented in Figure 10. These figures plot k vs. Re and for the same h/L values as before. Note that for almost all of the data the value of k shows little dependence on Re, although a slight increase in the magnitude of k with increasing Re seems to exist when considering all of the data. What is evident from Figures 9 and 10 is that for increasing h/L, with L^* fixed, k increases in magnitude. Thus, as h^* increases, the rate at which momentum is transported throughout the tank also increases. Also the data indicate that for increasing L^*, with h/L fixed, the magnitude of k increases.

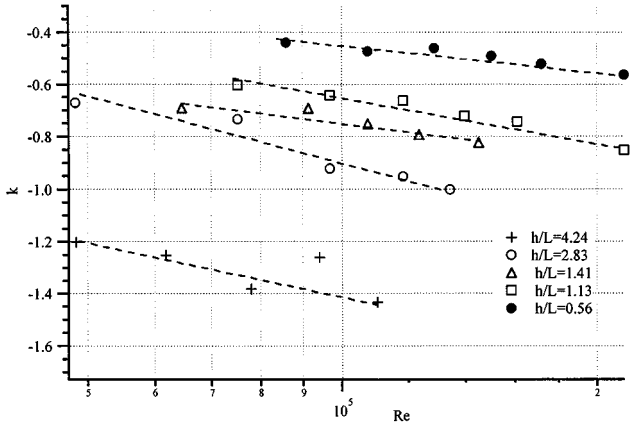

(a)

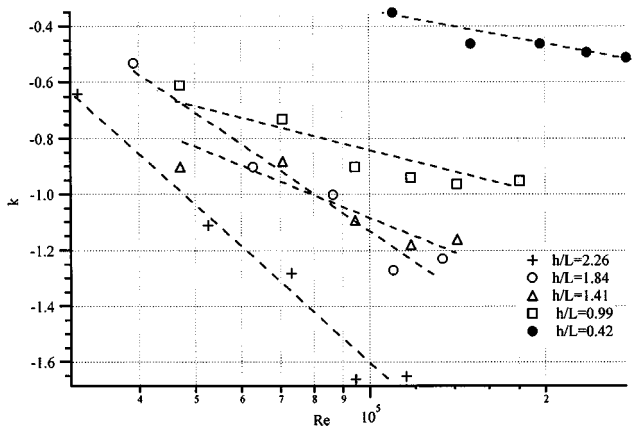

(b)

Figure 9. Decay exponent, k, vs. Reynolds number, Re, in the small tank ($H^* = 2.42$) for (a) $L^* = 0.39$, with h/L ranging from 0.56 to 4.24, and (b) $L^* = 0.67$, with h/L ranging from 0.42 to 2.26.

Tank-size effects and generalized relation for k

The k values for all of the bodies employed in the three tanks are plotted vs. the parameter $h^*L^{*3/2}$ in Figure 11. The Reynolds number was 10^5 for all of these cases. A least-square fit to the data suggests the relation

$$k = 1.25\sqrt{h^*L^{*3/2}}\,. \tag{11}$$

The agreement between the data from the three tanks is quite good with a correlation coefficient of 0.97 and an average difference between the fit expression and measurement of 8%. Note from the figure that the magnitude of k does not depend on H^*. This indicates that although the height of the tank is important in determining the steady-state value of C_m and in the total spin-up time, it does not affect the rate at which momentum is transported to the bulk fluid. This is affected only by the magnitude of L^* and h^*.

One question that arises when examining the data is Why does the torque decrease with a power-law form? This can be addressed by analysis of the turbulent kinetic energy. It was discussed in the section on the spin-up process that $C_m \sim v^{*2}$ throughout the spin-up process, although here we consider only the decay regime. Neglecting the conservative terms, and assuming isotropic and homogeneous turbulence in the tank, the turbulent kinetic energy equation can be written as

$$\frac{d\frac{3}{2}u'^2}{dt} + P = \Phi \tag{12}$$

where P and Φ represent the production and dissipation terms, and u' represents the turbulence intensity of the flow field. Assuming that u' scales like the rms of the velocity, v', and that both production and dissipation scale as v'^3/l, where l is the characteristic eddy length scale (Tennekes and Lumely, 1994), Eq. 12 can be written as

$$\frac{dv'^2}{dt} \sim \frac{v'^3}{l}\,. \tag{13}$$

The characteristic length scale of the large-scale eddies should scale like $v't$. Making this substitution and normalizing v' by ωL and t by l/ω, Eq. 13 can be expressed as

$$\frac{dv^{*2}}{v^{*2}} = k\frac{dt^*}{t^*}, \tag{14}$$

where the scaling argument can be replaced with an equality by multiplying by the unknown constant k. After integrating, this becomes

$$v^{*2} = t^{*k} + S, \tag{15}$$

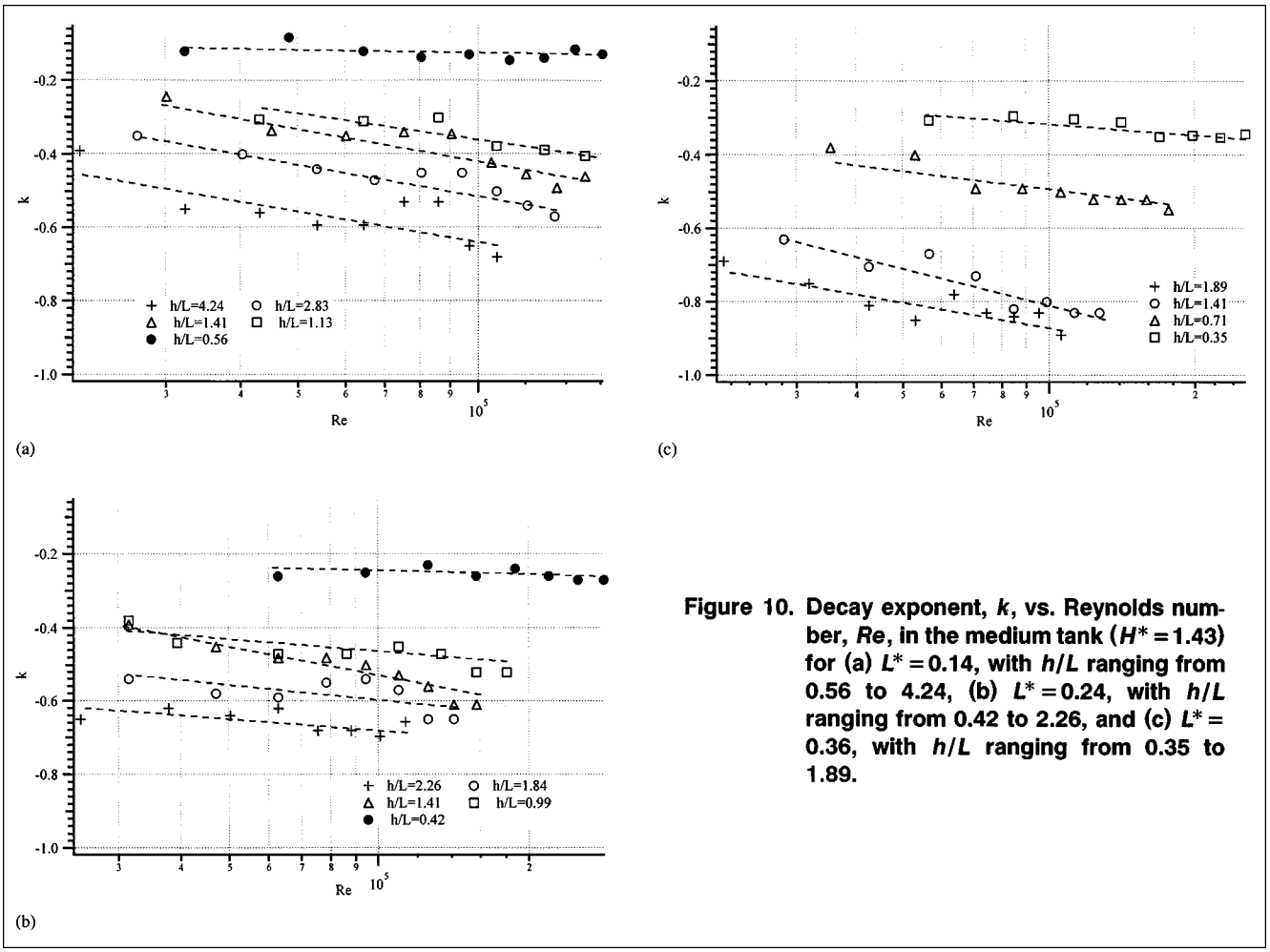

Figure 10. Decay exponent, k, vs. Reynolds number, Re, in the medium tank ($H^* = 1.43$) for (a) $L^* = 0.14$, with h/L ranging from 0.56 to 4.24, (b) $L^* = 0.24$, with h/L ranging from 0.42 to 2.26, and (c) $L^* = 0.36$, with h/L ranging from 0.35 to 1.89.

where S is the constant of integration. Recalling that $C_m \sim v^{*2}$, we can write

$$C_m \sim v^{*2} \sim t^{*k} + S. \tag{16}$$

The preceding scaling argument indicates that C_m should decay with a power-law relation, but the exponent k cannot be determined from the simple scaling analysis. Indeed, our data show that for all bodies investigated the decay of C_m in the decay regime was power-law in form. The decay exponent cannot be determined by scaling methods or other analytical approaches, but must be determined by either experiment or by computational modeling of the flow field. The data of Figure 11 show how this exponent depends on the geometric parameters for the impellers of interest based on all of our experimental data with $Re = 10^5$. For large body sizes, or $h^*L^{*3/2}$ of order 1, the power-law exponent k is close to -1, but decreases in magnitude to a value of about -0.25 when $h^*L^{*3/2} = 0.05$.

Description of C_m for Spin-Up from Rest

Previously, it was shown that during the buildup regime, the magnitude of C_m is only a function of h/L and does not depend on Re for the range from 10^4 to 10^5 (Maynes and Butcher, 2001). A physical description of the flow field was presented and empirical relations that describe the relationship were also presented. These are summarized here. If $h/L \leq 1.0$, than C_m is described by Eq. 17. Likewise if $h/L \geq 1.0$,

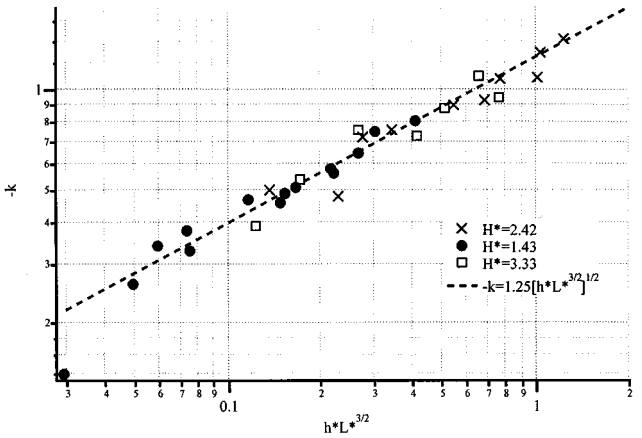

Figure 11. Decay exponent, k, vs. the parameter $h^*L^{*3/2}$ at $Re = 10^5$ for all h/L utilized in the three tanks.

then C_m is described by Eq. 18

$$C_m = 0.48 + 0.31\left(\frac{h}{L}\right) + 0.15\left(\frac{h}{L}\right)^2 \tag{17}$$

$$C_m = 0.48\left(\frac{h}{L}\right)^{-1} + 0.42. \tag{18}$$

Also the number of revolutions elapsed between initiation of motion and the point when the decay regime ends, or when decay starts, was quantified as a function of L^*, H^*, and h^*, in a similar manner to the steady-state time scale presented in the subsection on tank-size effects and generalized spin-up time scaling and Eq. 8. This time scale is given in Eq. 19

$$t^*_{bu} = 0.28\left[\left(\frac{L^*}{1+\frac{H^*}{2}}\right)^2\sqrt{\frac{h^*}{1+\frac{H^*}{2}}}\right]^{-0.89}. \tag{19}$$

In addition to Eqs. 9, 10, and 11, the preceding equations completely describe the spin-up from rest of a rotating impeller of square cross section and for the L^*, h^*, and H^* ranges shown in Table 1. Equations 17, 18, 19 and 9 are valid for the entire Re range explored (10^4–10^5). Although all of the physical behavior is similar at other Reynolds numbers, Eqs. 10 and 11 are based upon data with $Re = 10^5$, and modified relations are necessary to account for Reynolds number effects.

Conclusion

The significance of the data and relations presented in this article is that they enable prediction of the power requirements of an impeller as a function of time for the entire transient and steady-state process. Also prediction of the time required for mixing of momentum for a given mixing tank-impeller configuration is possible in addition to prediction of the time required for spin-up to steady state from rest. Furthermore the rate at which the turbulence level in the tank and the power necessary for constant rotation decreases with time during the spin-up process can be predicted based on the presented data and correlations. The data clearly show that if a decrease in mixing times is desirable for a certain process, increasing the aspect of the ratio of the impeller will facilitate this. Furthermore initial optimization of the mixing geometry (that is, total energy or actual time minimization), or scale-up to larger facilities, for a given application is possible with these relations without extensive testing of prototype systems. Although the presented expressions are for that of a simple impeller with a square cross section, similar behavior should exist for all radial-flow impellers located in the center of cylindrical tanks without baffles.

Notation

C_m = torque coefficient $(T/(1/2\,\rho\Omega^2L^4h)$
C_{me} = error in determining C_m
h = body height, m
h^* = nondimensional body height (h/R)
H = fluid height in tank, m
H^* = nondimensional tank height (H/R)
k = decay exponent
l = characteristic eddy size, m
l_x = characteristic tank-length scale, m
L = characteristic body length−impeller radius, m
L^* = nondimensional body length (L/R)
P = production of turbulent energy, m^2/s^3
R = tank radius, m
Re = Reynolds number ($\omega L^2/\nu$)
t = time (s)
t^* = nondimensional time (t^* = revolutions)
t^*_{bu} = revolutions until decay begins
t^*_{ss} = revolutions when steady state is attained
T = torque, N-m
u' = turbulence intensity, m/s
v' = rms of mean velocity, m/s
v^* = normalized rms velocity $[v'/(\omega L)]$
V = characteristic velocity (ωL, m/s)

Greek Letters

α = angular acceleration, $(1/s^2)$
Φ = dissipation of energy, m^2/s^3
η = ratio of h/L values of reference h/L value
λ = face length of bluff body (impeller), m
ν = kinematic viscosity, m^2/s
ρ = fluid density, kg/m^3
ω = angular rotation rate, 1/s
τ = normalized time scale describing spin-up time $t^*[L/l_x]^2$
ζ = ratio of torque to torque for a reference case

Literature Cited

Bertrand, J., J. P. Couderc, and H. Angelino, "Power Consumption, Pumping Capacity and Turbulence Intensity in Baffled Stirred Tanks: Comparison Between Several Turbines," *Chem. Eng. Sci.*, **35**, 2157 (1980).

Bujalski, W., A. W. Nienow, S. Chatwin, S., and M. Cooke, "The Dependency on Scale of Power Numbers of Rushton Disc Turbines," *Chem. Eng. Sci.*, **42**, 317 (1987).

Chudcek, M. W., "Impeller Power Numbers and Impeller Flow Numbers in Profiled Bottom Tanks," *Ind. Eng. Chem. Process Des. Dev.*, **24**, 858 (1985).

Ibrahim, S., and A. W. Nienow, "Power Curves and Flow Patterns for a Range of Impellers in Newtonian Fluids," *Trans. Inst. Chem. Eng.*, **73** (Part A), 485 (1995).

King, R. L., R. A. Hiller, and G. B. Tatterson, "Power Consumption in a Mixer," *AIChE J.*, **34**, 605 (1988).

Maynes, D., and M. Butcher, "Effect of Body Aspect Ratio and Tank Size on the Hydrodynamics of a Rotating Bluff Body During the Initial Spin-Up Period," *J. Fluids Eng.* (2001).

Maynes, D., J. C. Klewicki, and P. A. McMurtry, "Time Resolved Torque of Three Dimensional Rotating Bluff Bodies in a Cylindrical Tank," *J. Fluids Eng.*, **120**, 23 (1998).

Maynes, D., J. Klewicki, and P. McMurtry, "Spin-Up in a Tank Induced by a Rotating Bluff Body," *J. Fluids Mech.*, **388**, 49 (1999).

Nienow, A. W., and D. Miles, "Impeller Power Numbers in Closed Vessels," *Ind. Eng. Chem. Process Des. Dev.*, **10**, 41 (1971).

Oldshue, J. Y., *Fluid Mixing Technology*, McGraw-Hill, New York (1983).

Oliver, D. R., A. W. Nienow, R. J. Mitson, and K. Terry, "Power Consumption in the Mixing of Boger Fluids," *Chem. Eng. Res. Des.*, **62**, 123 (1984).

Papastefanos, N., and M. Stamatoudis, "Effect of Vessel and Impeller Geometry on Impeller Power Number in Closed Vessels for Reynolds Numbers Between 40 and 65000," *Chem. Eng. Res. Des.*, **67**, 169 (1989).

Rushton, J. H., E. W. Costich, and H. J. Everett, "Power Characteristics of Mixing Impellers Part I," *Chem. Eng. Prog.*, **46**, 395 (1950a).

Rushton, J. H., E. W. Costich, and H. J. Everett, "Power Characteristics of Mixing Impellers Part II," *Chem. Eng. Prog.*, **46**, 467 (1950b).
Rutherford, K., K. C. Lee, M. S. Mahmoudi, and M. Yianneskis, "Hydrodynamic Characteristics of Rusthon Impeller Stirred Vessels," *AIChE J.*, **42**, 332 (1996).
Sano, Y., and H. Usui, "Effects of Paddle Dimensions and Baffle Conditions on the Interrelations Among Discharge Flow Rate, Mixing Power and Mixing Time in Mixing Vessels," *J. Chem. Eng. Jpn.*, **20**, 399 (1987).
Tatterson, G. B., *Fluid Mixing and Gas Dispersion in Agitated Tanks*, McGraw-Hill, New York (1991).
Tennekes, H., and J. L. Lumley, *A First Course in Turbulence*, MIT Press, Cambridge, MA (1994).
Tiljander, P., and H. Theliander, "Power Consumption and Solid Suspension in Completely Filled Vessels," *Chem. Eng. Commun.*, **124**, 1 (1993).

Manuscript received Sept. 25, 2000, and revision received July 10, 2001.